Original article

Protective effect of Lonicerae Japonicae Flos extract against doxorubicin-induced myocardial injury in mice and the possible mechanisms

XIA Shicheng[1,3], WEI Huifang[1,3], HONG Weican[1,3], ZHANG Yuming[2,3], YIN Feiyang[1,3], ZHANG Yixin[1,3], ZHANG Linlin[2,3], GAO Qin[2,3], YE Hongwei[2,3]

[1]Department of Clinical Medicine, [2]Department of Physiology, [3]Key Laboratory of Basic and Clinical Research of Cardiovascular and Cerebrovascular Diseases, Bengbu Medical University, Bengbu 233030, China

Abstract: Objective To evaluate the protective effect of Lonicerae Japonicae Flos (LJF) extract against doxorubicin (DOX)-induced cardiotoxicity (DIC) and explore the possible mechanisms. **Methods** Network pharmacology, bioinformatics analysis and molecular docking were used to predict the targets of the core components of LJF. In a mouse model of DOX-induced myocardial injury, the protective effects of different doses of LJF extract were evaluated and the underlying mechanisms were explored by detecting the changes in mouse myocardial functions, myocardial enzymes, myocardial pathologies, and the expressions of inflammatory factors and pyroptosis-related proteins. **Results** The 10 core ingredients of LJF showed strong binding to AKT, EGFR, and GSK3β. In the animal experiment, the DOX-treated mice, compared with the sham-treated mice, had significantly decreased cardiac output, stroke volume, left ventricular ejection fraction, left ventricular fraction shorting, elevated serum levels of CK-MB and LDH, increased myocardial expressions of IL-18 and IL-1β, obvious myocardial damage, increased expression levels of NLRP3, caspase-1, GSDMD and GSDMD-N, and reduced expressions of EGFR, p-AKT and p-GSK3β proteins in the myocardial tissues. LJF treatment obviously improved myocardial function, decreased myocardial expressions of IL-18, IL-1β, NLRP3, caspase-1, GSDMD and GSDMD-N proteins, and increased the expressions EGFR, p-AKT and p-GSK3β proteins in DOX-treated mice. **Conclusion** LJF extract alleviates DOX-induced myocardial injury in mice possibly by reducing myocardial inflammation and pyroptosis *via* targeting EGFR, AKT and GSK3β to regulate the ErbB signaling pathway.

Keywords: network pharmacology; Lonicerae Japonicae Flos extract; doxorubicin; molecular docking; pyroptosis; ErbB signaling pathway

INTRODUCTION

Doxorubicin (DOX, also known as adriamycin) is a widely used drug for cancers with potent anti-cancer effects[1]. However, studies have shown that DOX can promote oxidative stress and inflammatory responses in the vital organs including the heart, liver, and kidneys as well as in the skeletal muscles [2-5]. DOX-induced cardiotoxicity (DIC) is one of its severe adverse effects following long-term continuous DOX treatment, and finding new drugs to reduce its cardiac toxicity can be of vital importance for improving the outcomes of cancer patients.

Received: 2025-03-04 **Accepted:** 2025-07-15

Supported by Anhui Provincial Funds for Excellent Scientific Research and Innovation Team (2022AH010083), 512 Talent Program of Bengbu Medical University (by51201102), and Innovation and Entrepreneurship Training Program for College Students (S202410367081, S202410367011, 202410367058, S202410367057).

Corresponding authors: YE Hongwei, associated professor, E-mail: yehongwei223@163.com; GAO Qin, PhD, professor, E-mail: bbmcgq@126.com.

The mechanism of DIC is complex and has not been fully elucidated. Experimental evidence suggests that GSDMD knockout can reduce the severity of DIC in DOX-treated mice[6]. DOX prompts cells to recruit IGF2BP by upregulating terminal differentiation-induced noncoding RNA, which increases NLRP3 expression and leads to the activation of caspase-1, cleavage of GMDSD-N, and the release of interleukin-1β (IL-1β) and IL-18[7]. These findings indicate that pyroptosis can be a potential pathogenetic mechanism of DIC.

Lonicerae Japonicae Flos (LJF) is the initial flowering or dried flower buds of *Lonicera japonica* Thunb (Caprifoliaceae). Apart from its use in traditional Chinese medicine, it has also been used as a "functional food" due to its effect of strengthening the immune system[8, 9]. Modern pharmacological research has identified more than 212 compounds in LJF, and these main active components are the material basis for the pharmacological effects of LJF[10]. Studies have shown that LJF has antioxidant, antiviral, anti-inflammatory, anti-allergic, heat-clearing and detoxifying, lipid-lowering, and immune regulatory effects[11-14]. A previous study demonstrated significant anti-inflammatory effects

of LJF[15]. Given that inflammation is a hallmark response of pyroptosis [16] and based on evidence from pharmacological research of LJF, we speculate that LJF has great potential for alleviating DIC through regulating pyroptosis. Currently few studies have been reported to examine the protective effect of LJF against DIC and the interactions between the main active components of LJF and the disease-related targets.

In this study, we used network pharmacology analysis and molecular docking to explore the core ingredients of LJF and their core targets that mediate the protective effect of LJF against DIC, and validated the findings in a mouse model DIC. Our finding may provide new insights into the mechanism by which LJF alleviates DOX-induced myocardial injury and pyroptosis.

METHODS

Screening of main active components in LJF

The chemical components of LJF were searched using the TCMSP database (https:/d. tcmsp-e. com/tcmsp. php). The main active components were selected based on conditions of an oral bioavailability above 30% and a drug-likeness beyond 0.18. The molecular structure diagrams of each main component were obtained from the TCMSP database, and their molecular structures were obtained using the NovoPro tool (https://novopro. cn/). The Swiss ADME platform was used for screening the compounds with a high GI absorption score and at least two Yeses for drug-likeness to identify the core ingredients.

Prediction of potential drug targets and construction of components-targets network

All the main active components of LJF were sequentially inputted into the Swiss Target Prediction platform to predict the related target genes of each core ingredient. The results were collected, organized, and visualized using Cytoscape3.7.2 software.

Acquisition of adriamycin-induced myocardial injury and pyroptosis related genes

The OMIM database (https://www. omim. org/) and the GeneCardard gene database (https://www. genecards. org/) were used simultaneously, with "adriamycin-induced myocardial injury" as the search term for retrieval and deduplication to obtain the genes related to DIC. In the GeneCardard gene database, "Pyroptosis" was used as the search term to obtain the genes related to cell pyroptosis.

Identification of the intersection genes and construction of the protein-protein interaction (PPI) network

The potential target genes of LJF-mediated pyroptosis against DOX-induced myocardial injury were identified by importing the target genes into the Venny2.1 website (https://bioinfogp. cnb. csic. es/tools/venny/) and drawing a Venn diagram. The intersection genes were then analyzed in the STRING database (https://cn. string-db. org/), with the species set to "Mus musculus". The TSV files were imported into Cytoscape3.7.2 software for visualization.

GO and KEGG analysis

Using the DAVID database (https://david. ncifcrf. gov/summary. jsp), the intersection genes of the drug components and diseases were imported for both GO functional annotation analysis and KEGG pathway enrichment analysis. The top-ranking gene functions and pathways from both analyses were visualized using bubble charts on the Microbial Information Platform (http://www.bioinformatics.com.cn/).

Selection of ligands and receptors and molecular docking

The core ingredients of LJF were identified using the TCMSP database and the small molecule structure files were obtained directly. The corresponding protein structures were obtained from PDB database (https://www. rcsb. org/) and docked with each of their target proteins using Autodock4 (A lower binding energy suggests stronger and more stable binding between the receptor and ligand). The molecular docking results were visualized using PyMol. The conformation with the lowest docking binding energy was input into the Protein-Ligand Interaction Profiler platform (https://plip-tool. biotec. tu-dresden. de/plip-web/plip/index) to obtain the interaction relationship and binding sites between the ligand and receptor. Visualization was performed using Cytoscape 3.7.2. The overall study design is illustrated by the flow chart in Fig.1.

Animals and treatments

Thirty male C57BL/6 mice, aged 6-8 weeks and weighing 18-22 g, were purchased from Hangzhou Ziyuan Laboratory Animal Technology Co., Ltd. (License No.: SCXK [Zhejiang] 2019-0004) and housed in a standard clean environment (22-25 °C) with free access to food and a 12 h dark/light cycle. During the experiment, the ethical guidelines established by Bengbu Medical University were strictly followed (Animal Ethics Approval No.: [2022] No. 024). After a week of adaptive feeding, the mice were randomized into 5 groups: Sham group, where the mice were given an equivalent amount of saline through tail vein injection and gavage with distilled water; DOX group, where the mice were given 2.5 mg/kg doxorubicin hydrochloride (Dalian Meilun Biotechnology Co., Ltd) *via* tail vein injection on the 3rd, 5th, 10th, and 12th days (with a cumulative dose of 10 mg/kg[17]) for DIC modeling and treatment with distilled water via gavage; and LJF

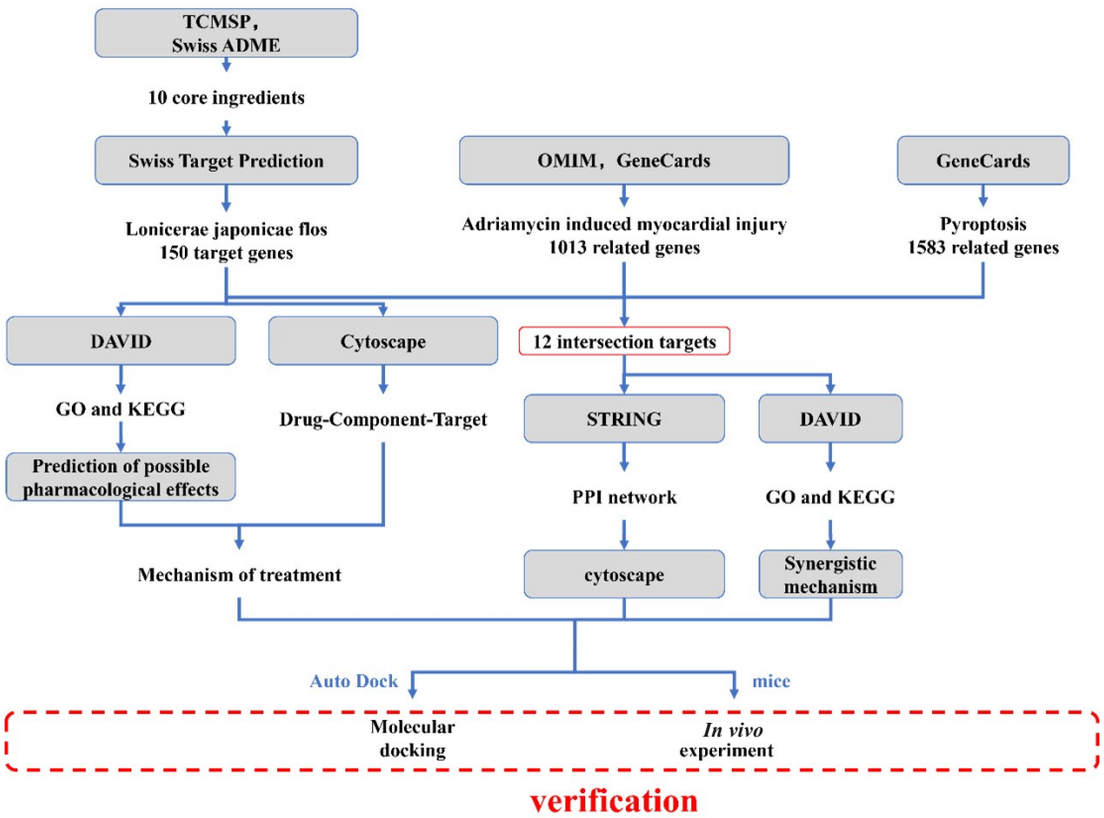

Fig.1 Flow chart of the study design.

extract treatment groups at low, medium, and high doses, where the mouse models of DIC were gavaged daily with LJF extract (LJF, Xinxiang Bokai Biotechnology Company) at 0.2, 0.4, and 0.8 g/kg, respectively, starting from two days prior to the first DOX injection for DIC modeling for a total of 2 weeks[14].

Echocardiography

Two days after the last DOX injection, the mice were anesthetized with isoflurane and immobilized for measurement of the M-curves along the short axis of the papillary muscle and at the level of the left ventricular section using a Vevo 2100 microultrasound imaging system (VisualSonics, Canada). Cardiac output (CO; mL/min), stroke volume (SV; μL), left ventricular ejection fraction (LVEF; EF%) and left ventricular fractional shortening (LVFS; FS%) of the mice were measured. The ejection fraction was calculated as: LVEF (EF%) = (LVDV − LVSV)/LVDV×100%; the fractional shortening as: LVVFS (FS%)=(LVDD−LVSD)/LVDD × 100%.

Histological examination of myocardial tissues

After the last gavage treatment, the mice were fasted for 12 h, anesthetized for collection of blood samples, and euthanized by cervical dislocation for harvesting the heart specimens, which were immediately preserved at −80 ℃. For preparing paraffin sections, the mouse hearts were fixed with 4% paraformaldehyde for 48 h, dehydrated, embedded in paraffin, and sliced into 5 μm slices. For HE staining, the tissue sections were treated with the pre-treatment solution for 1 min, and stained with hematoxylin solution for 5 min. After washing, the slices were placed in a differentiation solution for differentiation and cleaning, followed by treatment with a reblueing solution and rinsed with water. After dehydration with 95% alcohol for 1 min, the slices were stained with eosin solution for 15 s. Gradient anhydrous ethanol was used for further dehydration, followed by transparency treatment with n-butanol and xylene. Finally, the slices were mounted with neutral resin and observed under an optical microscopy (OLYMPUS, Tokyo, Japan).

Myocardial enzyme assay

The mice were anesthetized with isoflurane, and orbitol blood samples were collected in centrifuge tubes. After 30 min of blood clotting, serum was isolated by centrifuging of the blood samples at 3000 r/min at 4 ℃ for 10 min. Serum levels of creatine kinase-MB (CK-MB) and lactate dehydrogenase (LDH) were detected using CK-MB assay kit and LDH assay kit (Nanjing Jiancheng Bioengineering Institute) following the manufacturer's instructions.

Enzyme-linked immunosorbent assay (ELISA)

The levels of pyroptosis-related inflammatory cytokines interleukin-18 (IL-18) and IL-1β in mouse heart homogenate were measured using ELISA kit (Jiangsu

Jingmei Biotechnology Co., Ltd) following the manufacturer's instructions. Briefly, the myocardial tissue from each mouse (20 mg) was homogenated and centrifuged at 3000 r/min for 10 min at 4 ℃, and the protein concentration in the supernatant was determined using the BCA method. In the standard sample wells and test sample wells, 50 μL of the standard sample and 10 μL of the test sample were added, respectively, followed by addition of 100 μL of horseradish peroxidase (HRP)-labeled detection antibody. The mixture was incubated at 37 ℃ for 60 min, and the liquid in the wells was discarded, after which 50 μL of substrate A and substrate B was added to each well. After incubation in the dark at 37 ℃ for 15 min, 50 μL of stop solution was added. The absorbance value at 450 nm of each well was measured using a microplate reader (BioTek instruments Inc, Serial#:121221C). The content of IL-18 and IL-1β in the myocardial tissue sample were calculated according to the standard curves.

Western blotting

The total protein from the heart tissues were isolated using RIPA lysis buffer on ice, and the supernatants were collected after centrifugation. The protein concentrations were measured using a BCA protein assay kit BCA kit (Epizyme Biomedical Technology Co., Ltd). Equal amounts of the samples from each group were loaded on 10% SDS-PAGE to separate the proteins, which were transferred to a polyvinylidene difluoride membrane. The membranes were blocked with 5% skimmed milk (dissolved in Tris-buffered saline with Tween 20) and then incubated with the primary antibodies against NLRP3 (1: 2000; Proteintech), caspase-1 (1: 2000; Affinity Bioscience), GSDMD (1:1000; Cell Signaling Technology), GSDMD-N (1:1000; Abcam), EGFR (1:2000; Proteintech), AKT (1: 5000; Proteintech), p-AKT (1: 2000; Proteintech), GSK3β (1: 1000; Proteintech), p-GSK3β (1: 2000; Proteintech), and GAPDH (1: 50 000; Biosharp) overnight at 4 ºC. After incubation with the corresponding secondary antibody (1:5000; Proteintech), the protein blots were visualized with enhanced chemiluminescence BeyoECL Star (Beyotime, Shanghai, China), and the chemiluminescent signals were captured using the ChemiDoC XRS+ system. The relative intensity of the chemiluminescent signals was quantified using the ImageJ software.

Statistical analysis

All the data in this study were statistically analyzed using SPSS 22.0 software. The measurement data are presented as *Mean±SD*. For data with normal distribution and homogeneity of variance, comparisons among the groups were performed using one-way ANOVA, while multiple pairwise comparisons were conducted with LSD method. For data that failed the homogeneity of variance test, Kruskal-Wallis test was used for comparisons among multiple groups. A P value less than 0.05 was considered to indicate a statistically significant difference.

RESULTS

Main active components and the core ingredients of LJF

A total of 23 main active components were screened from LJF, which all had an oral bioavailability above 30% and a drug-likeness above 0.18, and 10 core ingredients were identified (Tab.1).

GO and KEGG enrichment analyses of target genes of active ingredients in LJF

Using the Swiss Target Prediction platform, a total of 150 target genes of the core ingredients of LJF were identified (Fig. 2A), and the top 10 target genes ranked based on their Degree values are listed in Tab.2.

The target genes of the core ingredients in LJF were imported into the DAVID bioinformatics database, followed by GO and KEGG enrichment analysis. The top 10 terms according to the P values in Biological Process (BP), Cell Component (CC), and Molecular Function (MF) and the top 20 signal pathways in terms of the P values visualized using Microbial Bioinformatics are shown in Fig.2B and 2C.

Intersection genes and construction of PPI network

A total of 1013 genes related to adriamycin-induced myocardial injury and 1583 pyroptosis-related genes were retrieved, summarized using the OMIM database and the GeneCardard gene database. The Venn diagram of the target genes of LJF core ingredients and the disease target genes showed 12 intersection genes (Fig. 3A). The PPI network constructed based on these intersection genes highlights 12 targets: *Akt*, *Mapk14*, *Stat3*, *Egfr*, *Gsk3b*, *Mmp9*, *Casp1*, *Ptgs2*, *Cdk1*, *Nos2*, *Hdac6*, *Abl1* (Fig.3B).

GO and KEGG enrichment analysis of the intersection genes

GO and KEGG enrichment analyses were performed for the intersection genes, resulting in the top 10 terms in BP, CC, and MF (Fig. 4A) and the top 20 signaling pathways (Fig. 4B). The key targets *Akt*, *Egfr* and *Gsk3b* are all components of the ErbB signaling pathway (Fig.4C).

Molecular docking and visualization

In molecular docking studies, the binding energy is a key indicator for evaluating the strength of receptor-ligand binding, and a binding energy below -5 kJ·mol^{-1} indicates a strong binding between the target genes and

Tab.1 Main active components and the core ingredients in Lonicerae Japonicae Flos (LJF)

Mol ID	Molecule	OB	DL	Core ingredients
MOL000006	luteolin	36.16	0.25	Yes
MOL000098	quercetin	46.43	0.28	Yes
MOL000358	beta-sitosterol	36.91	0.75	No
MOL000422	kaempferol	41.88	0.24	Yes
MOL000449	Stigmasterol	43.83	0.76	No
MOL001494	Mandenol	42	0.19	No
MOL001495	Ethyl linolenate	46.1	0.2	No
MOL002707	phytofluene	43.18	0.5	No
MOL002773	beta-carotene	37.18	0.58	No
MOL002914	eriodyctiol (flavanone)	41.35	0.24	Yes
MOL003006	(-)-(3R,8S,9R,9aS,10aS)-9-ethenyl-8-(beta-D-glucopyranosyloxy)-2,3,9,9a,10, 10a-hexahydro-5-oxo-5H,8H-pyrano[4,3-d]oxazolo[3,2-a]pyridine-3-carboxylic acid_qt	87.47	0.23	Yes
MOL003014	secologanic dibutylacetal_qt	53.65	0.29	Yes
MOL003036	ZINC03978781	43.83	0.76	No
MOL003044	chryseriol	35.85	0.27	Yes
MOL003059	kryptoxanthin	47.25	0.57	No
MOL003062	4,5'-Retro-.beta.,.beta.-Carotene-3,3'-dione, 4',5'-didehydro-	31.22	0.55	No
MOL003095	5-hydroxy-7-methoxy-2-(3,4,5-trimethoxyphenyl)chromone	51.96	0.41	Yes
MOL003101	7-epi-Vogeloside	46.13	0.58	No
MOL003108	caeruloside C	55.64	0.73	No
MOL003111	centauroside_qt	55.79	0.5	Yes
MOL003117	niceracetalides B_qt	61.19	0.19	Yes
MOL003124	XYLOSTOSIDINE	43.17	0.64	No
MOL003128	dinethylsecologanoside	48.46	0.48	No

OB: Oral bioavailability; DL: Drug-likeness.

Tab.2 Top 10 target genes based on degree values

Gene name	Betweenness unDir	Closeness unDir	Degree unDir
Akt1	3568.885	0.004608	83
Stat3	1519.647	0.004149	66
Pparg	1574.181	0.004032	57
Gsk3b	2449.064	0.004082	55
Egfr	632.9566	0.003906	54
Esr1	1016.3	0.003861	50
Mmp9	1198.398	0.003861	49
Hif1a	515.0458	0.003876	49
Ptgs2	971.437	0.003861	49
Mapk14	546.9512	0.003831	48

the core ingredients. We conducted molecular docking of the core ingredients luteolin (MOL000006), quercetin (MOL000098), kaempferol (MOL000422), eriodyctiol (flavanone) (MOL002914), (-)-(3R, 8S, 9R, 9aS, 10aS)-9-ethenyl-8- (beta-D-glucopyranosyloxy) -2, 3, 9, 9a, 10, 10a-hexahydro-5-oxo-5H, 8H-pyrano[4, 3-d]oxazolo [3, 2-a]pyridine-3-carboxylic acid_qt (MOL003006), secologanic dibutylacetal_qt (MOL003014), chryseriol (MOL003044), 5-hydroxy-7-methoxy-2-(3, 4, 5-trimethoxyphenyl) chromone (MOL003095), centauroside_qt (MOL003111), and ioniceracetalides B_qt (MOL003117) with the core target genes AKT, EGFR, and GSK3β in the PPI network, and selected those with low binding energies for compound docking conformations. The docking results indicated that most of the core ingredients of LJF were stably docked with the 3 target genes (AKT, EGFR, and GSK3β) in the ErbB signaling pathway (Tab. 3 and Fig. 5A). The analysis identified a total of 36 binding sites for AKT, 46 interaction force sites for EGFR, and 40 interaction force sites for GSK3β. At the same time, the LYS-268 site of AKT, the ARG-776 site of EGFR, and the PHE-360 site of GSK3β are common sites that interact with multiple components (Fig. 5B-D), indicating that the protective effects of LJF against DIC and pyroptosis are likely mediated by the ErbB signaling pathway.

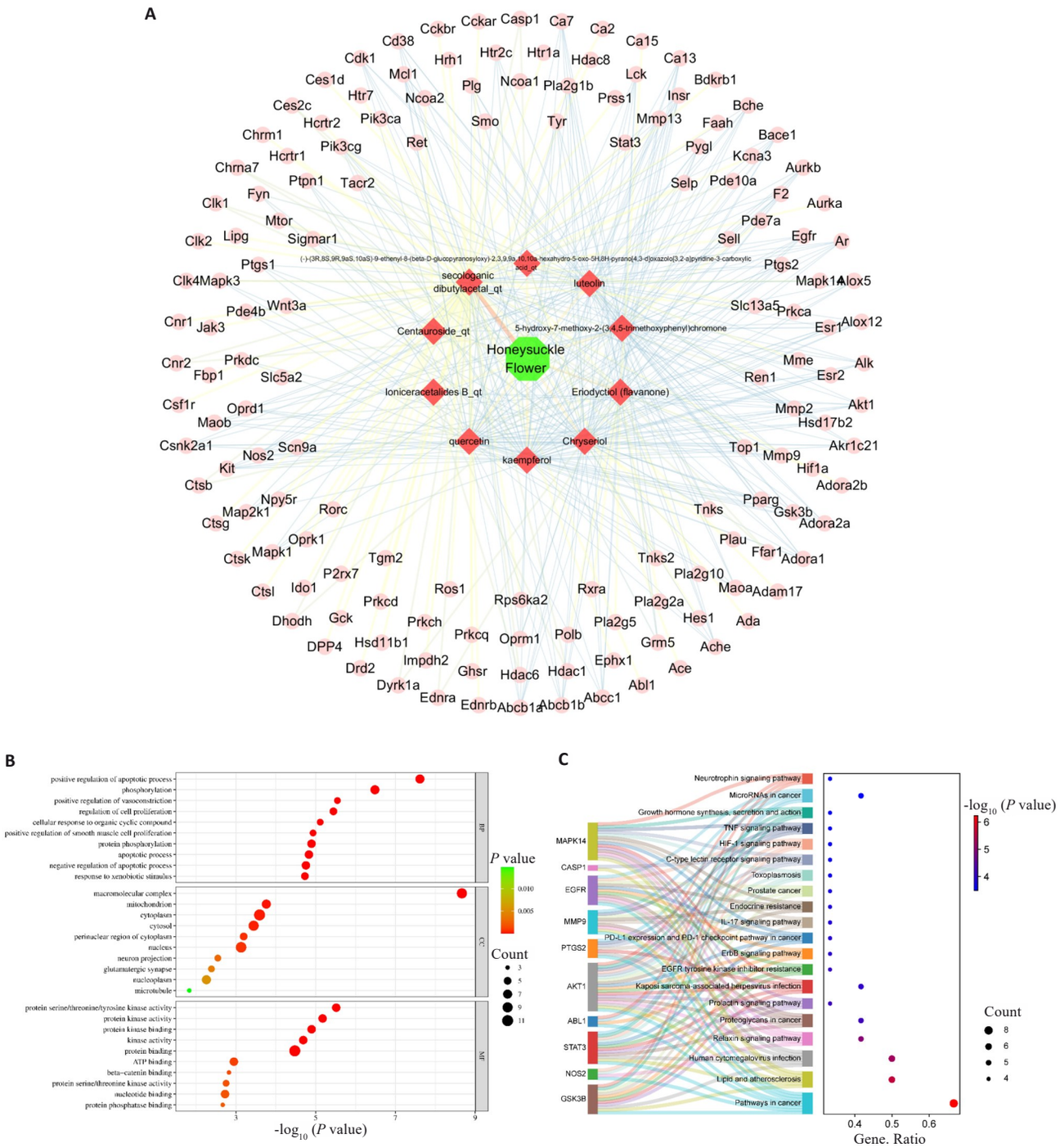

Fig. 2 Target genes of the core ingredients in LJF (**A**) and GO enrichment analysis (**B**) and KEGG enrichment analysis (**C**) of these targets.

Echocardiographic findings in DIC mice

Fig. 6 shows echocardiographic findings of the mice and the cardiac function parameters including CO, SV, EF, and FS in the 5 groups. Compared with those in the Sham group, the DOX-treated mice showed significantly decreased CO, SV, EF, and FS. In DOX-treated mice, treatments with LJF extract at the 3 doses all significantly increased CO level (P<0.01 or 0.0001) and SV level (P<0.05 or 0.01). LJF extract at the low and high doses significantly increased LVEF (P<0.01 or 0.001) and LVFS (P<0.01) in DOX-treated mice. These results demonstrate the protective effects of different doses of LJF against DIC in mice.

Histopathological findings in mouse myocardial tissues

Fig. 7 shows the histopathological findings in the myocardial tissues of the mice in each group. In the Sham group, the myocardial structure was intact, and all the cells were evenly stained (the cytoplasm appears pink and the nuclei are blue-purple). In DOX group, the

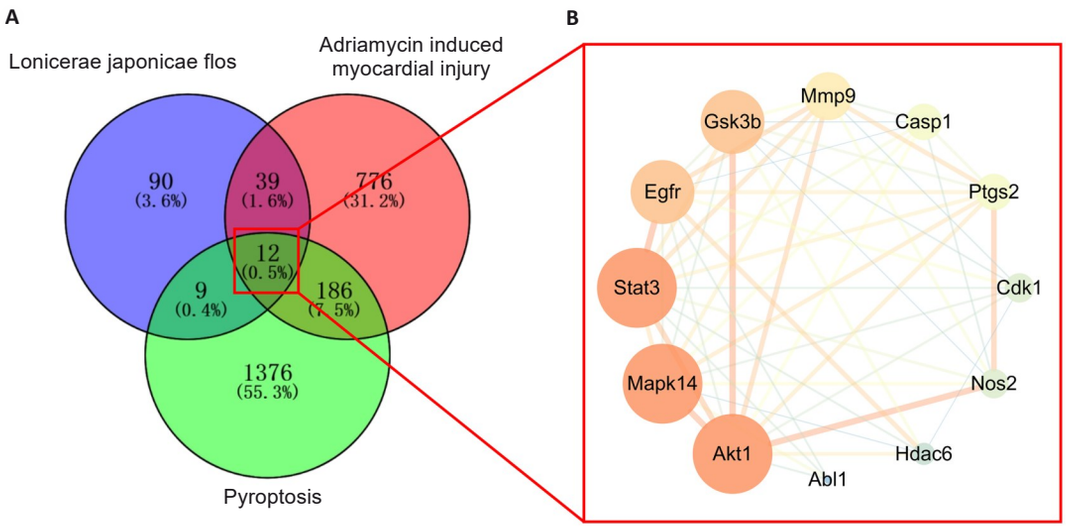

Fig.3 Venn diagram of the target genes of LJF, adriamycin-induced myocardial injury and pyroptosis-related targets (**A**) and the intersection genes network diagram (**B**).

myocardial tissues showed disordered arrangement of the cardiomyocytes with obvious cell edema and vacuoles, blood cell exudation, and infiltration of inflammatory cells. These myocardial pathologies were alleviated in LJF treatment groups, where obvious reductions of myocardial cell swelling, vascular dilation, and red blood cell exudation were observed.

Myocardial enzymes and inflammatory factors in mice

Compared with those in the Sham group, the serum levels of CK-MB and LDH in DOX group were significantly increased (P<0.0001), which were effectively lowered by treatment with LJF extract at low, medium, and high doses (P<0.01 or 0.0001; Fig.8A and B). The DOX-treated mice had significantly increased myocardial IL-18 and IL-1β levels as compared with those in the Sham group (P<0.0001), and treatments with LJF extract at the 3 doses all significantly decreased IL-18 and IL-1β levels in the mouse models (P<0.05 or 0.01; Fig.8C and D).

Results of Western blotting

The expression levels of NLRP3, caspase-1, GSDMD, GSDMD-N, EGFR, AKT, GSK3β, p-AKT and p-GSK3β in the myocardial tissues were detected by Western blotting. In DOX group, the relative protein expression levels of NLRP3, caspase-1, GSDMD, and GSDMD-N increased (P<0.05, 0.01 or 0.001) while EGFR, p-AKT/AKT and p-GSK3β/GSK3β protein expression levels decreased significantly (P<0.01 or 0.001) in the myocardial tissues as compared with those in the Sham group. High-dose LJF treatment significantly decreased the protein expression levels of NLRP3, caspase-1, GSDMD and GSDMD-N (P<0.05 or 0.01) and increased the expression levels of EGFR, p-AKT/AKT and p-GSK3β/GSK3β (P<0.05 or 0.01) in the DOX-treated mice (Fig. 9). These results demonstrate that DOX significantly inhibited the ErbB signaling pathway and induced pyroptosis in mouse myocardial tissues, and these changes were partly reversed by LJF treatment.

DISCUSSION

The molecular pathogenesis of DIC is very complex and may involve oxidative stress, Ca^{2+} overload, inflammation, pyroptosis, ferroptosis, apoptosis, and aging, etc [18]. Traditional Chinese herbal medicines have attracted increasing attention due to their advantages such as low toxicity, fewer side effects, and multi-target effects. Using network pharmacological analysis, we identified 10 core ingredients of LJF absorbed in the stomach and predicted 150 potential target genes. The top 10 target genes include *Akt1*, *Stat3*, *Pparg*, *Gsk3b*, *Egfr*, *Esr1*, *Mmp9*, *Hif1a*, *Ptgs2*, and *Mapk14*, and some of them were reported to be closely involved in pyroptosis[19-23]. We thus speculate that the pharmacological effects of LJF are mediated through its multiple components, targets, and pathways that are coordinated to regulate pyroptosis. We further screened the genes related to DOX-induced myocardial injury and pyroptosis, intersected them with the target genes of the core ingredients of LJF, and obtained 12 target genes. Among them, the top 5 target genes *Akt1*, *Mapk14*, *Stat3*, *Egfr*, and *Gsk3b* are enriched primarily in the relaxin, prolactin, ErbB, and IL-17 signaling pathways.

The ErbB signaling pathway activates its related signaling pathways by forming cascade signals to improve the myocardial microenvironment and regulate cardiac inflammation, oxidative stress, and necrotic apoptosis[24]. ErbB-1 (also known as EGFR) is an important factor in the ErbB signaling pathway, which, by activating the downstream PI3K-AKT signaling

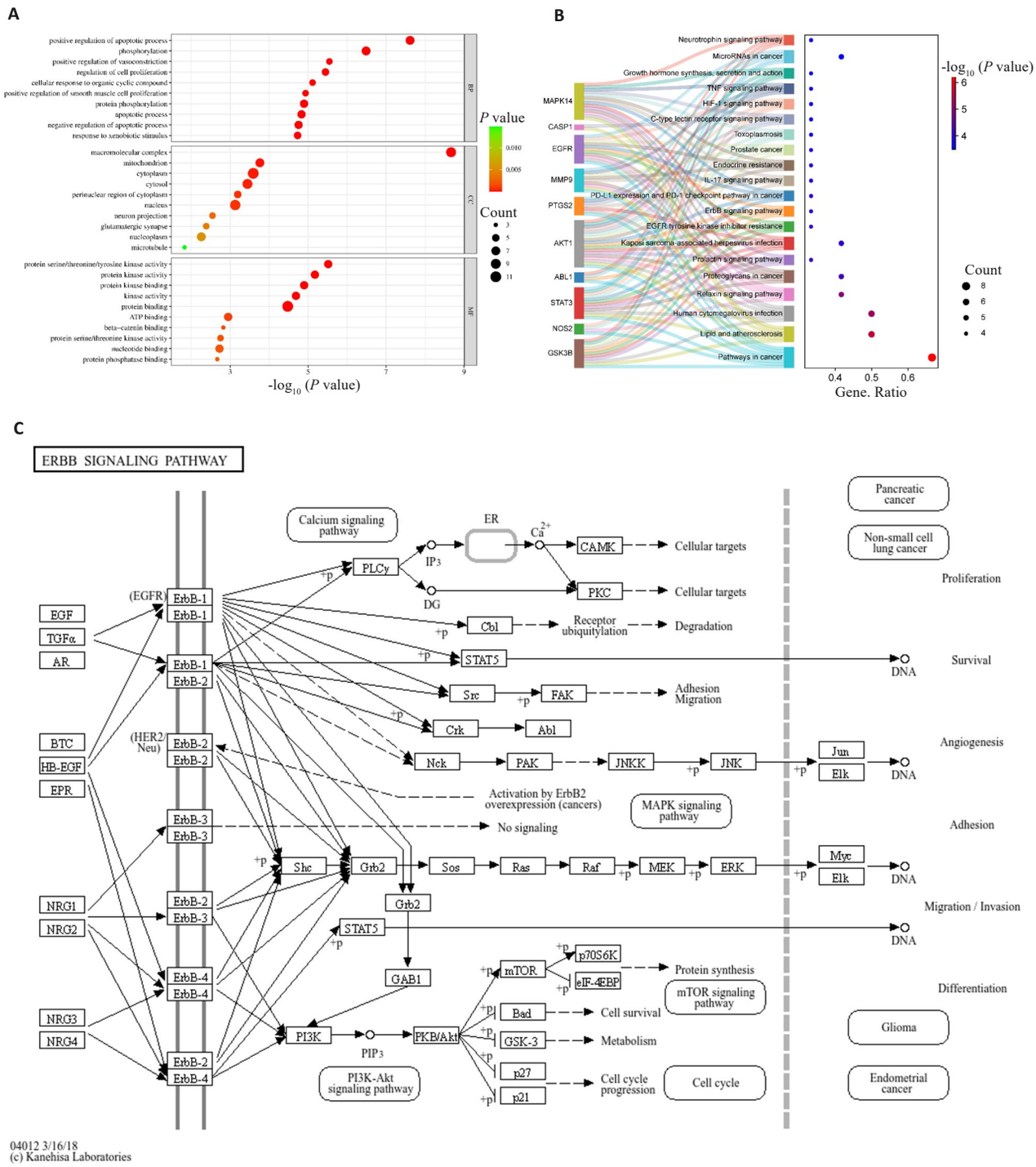

Fig. 4 GO enrichment analysis (**A**) and KEGG enrichment analysis (**B**) of the intersection genes and diagram of the ErbB signaling pathway (**C**).

pathway, results in the activation of GSK3β. Studies have shown that cryptotanshinone improves DIC by targeting the Akt-GSK3β-mPTP pathway [25], and relaxin signaling, in addition to the ErbB signaling pathway, reduces cell pyroptosis by inhibiting NLRP3 via activating PI3K/Akt and regulating MAPK phosphorylation[26]. In contrast, IL-17 signaling promotes pyroptosis and fibrosis, but its inhibition suppresses both pro-apoptotic and pro-fibrotic cascades, resulting in reduced myocardial pyroptosis and collagen deposition[27, 28]. *Akt1*, *Egfr*, and *Gsk3b* are important components of the ErbB signaling pathway, which has been identified as an potential therapeutic target for cancer and heart-related diseases[29]. Currently studies addressing the role of ErbB signaling pathway in heart diseases remain scarce, but given its regulatory effect on cell apoptosis, we speculate that the ErbB signaling pathway may play an important role in DIC and hence serves as a potential therapeutic target.

To explore the mechanisms of LJF components for

Tab.3 Binding energy of the core ingredients of LJF with their core target genes

Mol ID	Binding energy (kJ·mol^{-1})		
	EGFR	AKT1	GSK3β
MOL000006	-5.51	-6.98	-5.83
MOL000098	-6.07	-6.96	-5.8
MOL000422	-5.87	-7.41	-6.45
MOL002914	-5.46	-5.36	-5.23
MOL003006	-5.81	-5.92	-5.06
MOL003014	-2.13	-3.02	-2.25
MOL003044	-4.83	-7.2	-5.66
MOL003095	-5	-6.82	-5.49
MOL003111	-6.29	-3.99	-3.37
MOL003117	-5.91	-5.31	-4.8

alleviating DIC, we conducted molecular docking studies of the target genes in the ErbB signaling pathway. The results revealed a strong receptor-ligand binding affinity, especially for kaempferol, chryseriol, luteolin, and quercetin. These components, all having similar structures with multiple hydroxyl groups and aromatic ring structures, are capable of forming hydrogen bonds and hydrophobic interactions at the analogous sites on the target genes. In their conformations, AKT, EGFR, and GSK3β all show multiple binding sites for the components of LJF with relatively low binding energies, indicating a potential multi-site competition-pharmacodynamic change in a genuine cellular environment to influence both the magnitude and duration of drug efficacy[30]. Notably, the formation sites for the interaction forces are observed at LYS-268 of AKT (8 interaction forces), ARG-776 of EGFR (5 interaction forces), and PHE-360 of GSK3β (7 interaction forces), suggesting the possibility of their competitive binding to the same protein-binding pocket when selecting the conformation with the lowest binding energy for each component. Nevertheless, due to their structural similarities, different components might induce a "structure overlap-site sharing-functional adjustment" mechanism. This could lead to either functional synergy or antagonism to affect the protein's activation status or ability to bind downstream substrates, thereby amplifying or diminishing the pharmacological activities of LJF [31].

To validate the results of network pharmacology, we tested the effects of different doses of LJF extract in a mouse model of DOX-induced myocardial injury. We found that treatment with LJF at the low, medium and high doses all significantly improved CO, SV, LVEF and LVFS in the mouse models, resulting also in lowered serum levels of CK-MB and LDH, lessened myocardial pathologies, and reduced inflammatory cell infiltration in the myocardial tissues. These results demonstrate that LJF can alleviate cardiotoxicity caused by DOX. In the event of pyroptosis, the cells undergo membrane lysis with massive production of inflammatory factors [32], and the pattern recognition receptor NLRP3 recognizes these changes to form an NLRP3 inflammasome with ASC connected by pro-proteinase-1, which produces activated caspase-1 [33]. At the same time, pro-IL-1β and pro-IL-18 are cleaved by caspase-1 to form activated IL-1β and IL-18. Caspase-1 can cleave Asp275 (mouse Asp276) of GSDMD [34], releasing its self-inhibiting GSDMD-N domain and stimulating its pore-forming function [35]. Previous studies have shown that pyroptosis is involved in DIC [7,36,37], but whether LJF can regulate pyroptosis to alleviate DIC awaits further confirmation.

We found in the animal experiment that LJF at 0.8 g/kg produced a better effect for alleviating DIC. We therefore chose the dose of 0.8 g/kg in the subsequent experiments to explore whether LJF alleviates DIC through the target genes *Egfr*, *Akt*, and *Gsk3b* in the ErbB signaling pathway. In the DOX-treated mice, treatment with LJF significantly reduced the expression of EGFR protein, phosphorylation levels of AKT and GSK3β, and the expression levels of IL-18 and IL-1β and the key factors in the classical pyroptosis pathway (NLRP3, caspase-1, GSDMD, and GSDMD-N) in the myocardial tissue. These results suggest that LJF can inhibit myocardial cell pyroptosis through inhibiting EGFR, AKT and GSK3β expressions to alleviate DOX-induced myocardial injury, and provide experimental evidence that verifies the predictive results of network pharmacology.

Conclusion

In summary, we explored the possible mechanisms underlying the protective effect of LJF against DIC using network pharmacology, molecular docking, and a mouse model of DOX-induced myocardial injury. LJF extract alleviates DIC possibly through its core ingredients that inhibit cell pyroptosis by regulating the ErbB signaling

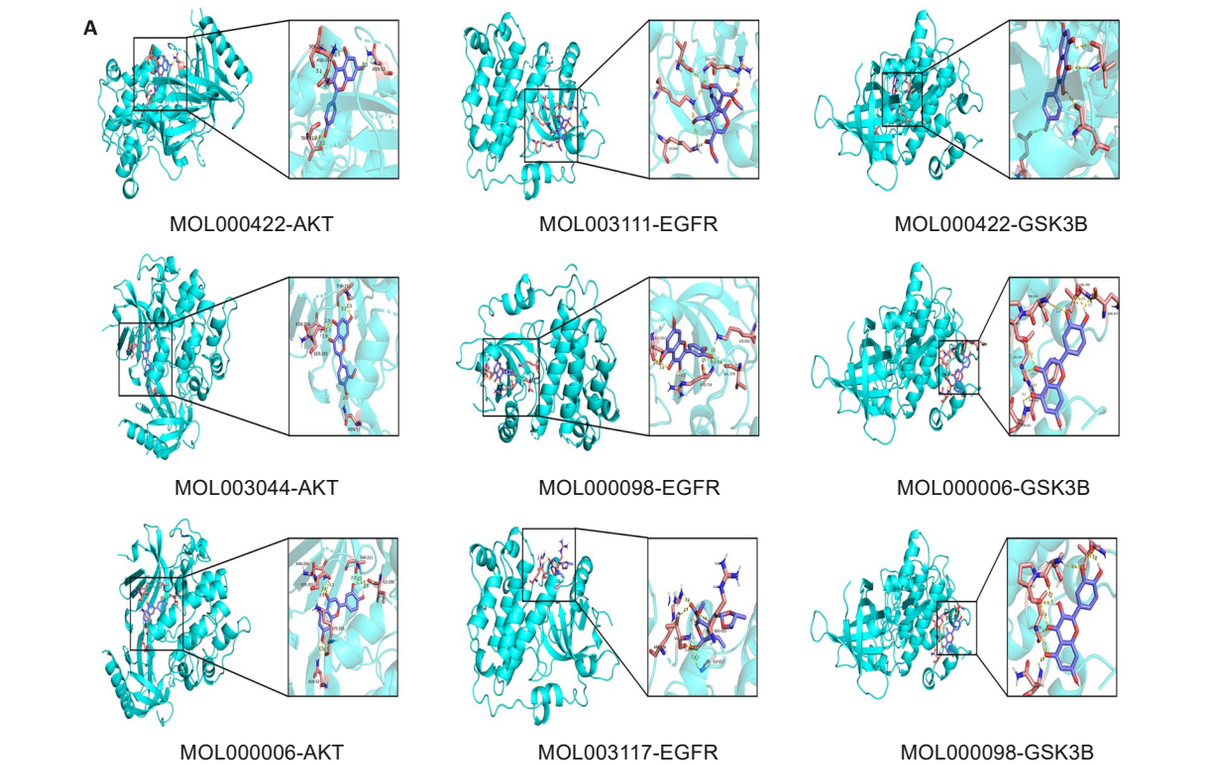

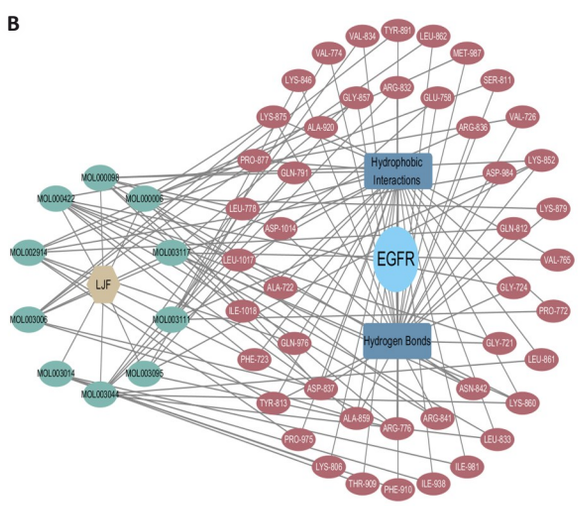

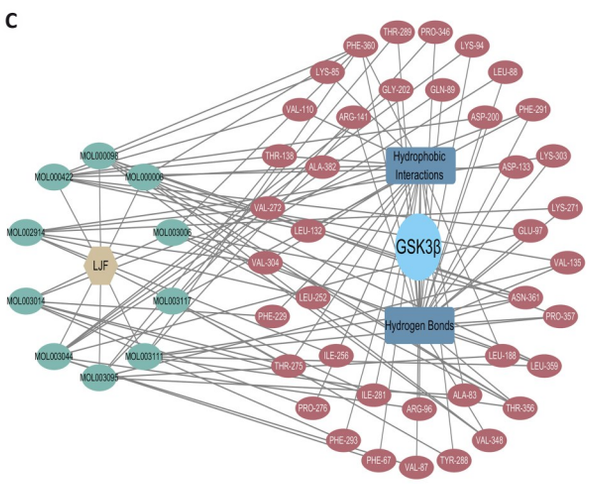

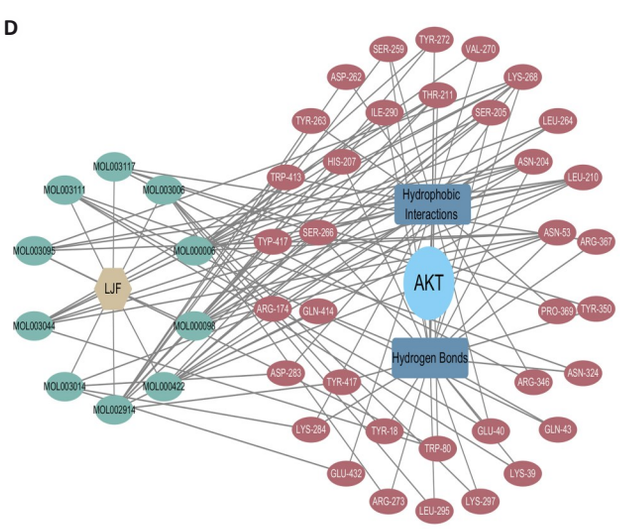

Fig. 5 Molecular docking study of the core ingredients of LJF with their core target genes and their interactions. **A**: Part of the results of molecular docking results. **B**: The "drug-component-site of action-type of action-protein" network of EGFR. **C**: The "drug-component-site of action-type of action-protein" network of GSK3β. **D**: The "drug-component-site of action-type of action-protein" network of AKT.

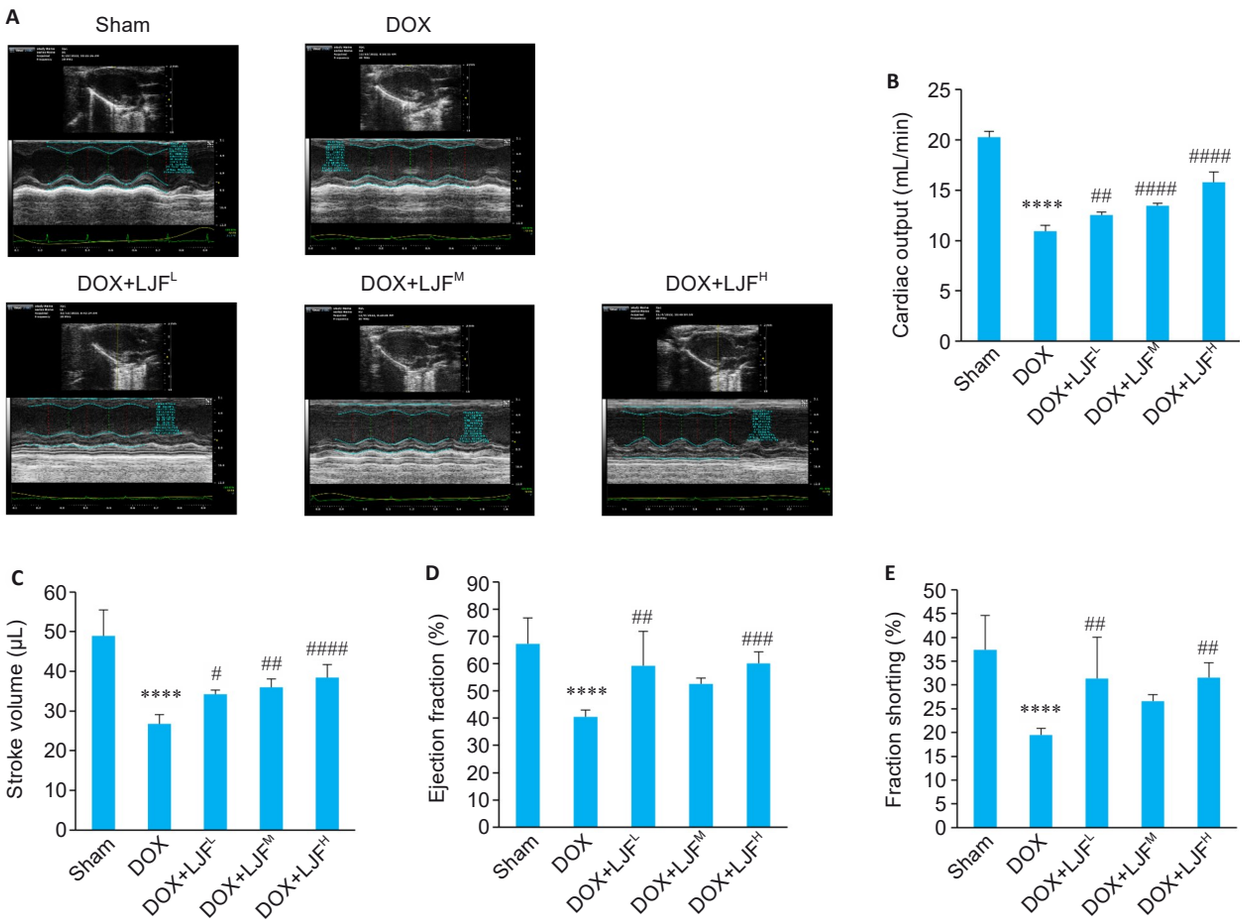

Fig. 6 Cardiac echocardiographic findings of the mice and the cardiac function parameters of the mice in each group. **A**: Cardiac echocardiography of the mice in each group. **B**: Comparison of cardiac output of the mice among the 5 groups. **C**: Comparison of the stroke volume of the mice among the 5 groups. **D**: Comparison of ejection fraction of the mice among the 5 groups. **E**: Comparison of fraction shorting of the mice among the 5 groups. Data are presented as *Mean±SD* (*n*=6). ****P<0.0001 *vs* Sham group; $^{\#}P$<0.05, $^{\#\#}P$<0.01, $^{\#\#\#}P$<0.001, $^{\#\#\#\#}P$<0.0001 *vs* DOX group.

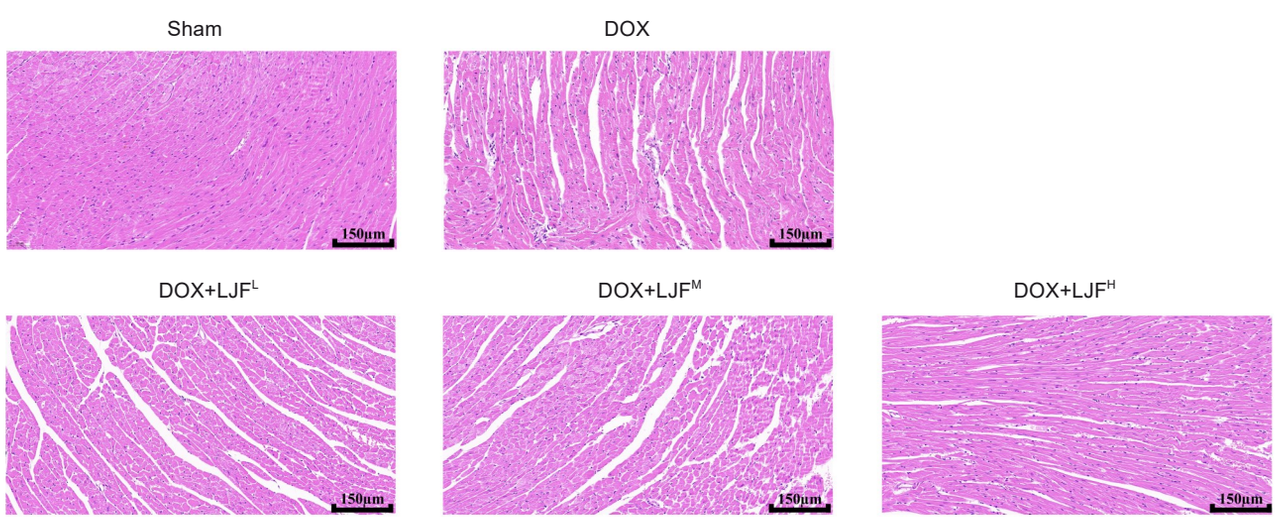

Fig.7 HE staining of myocardial tissue in each group of mice (Original magnification: ×20).

pathway via binding with EGFR, AKT, and GSK3β. This finding provides new insights into the regulatory mechanisms of pyroptosis based on which new treatment strategies for DIC can be devised. But due to the complexity of LJF components and the diversity of action sites, further investigations of the therapeutic mechanisms of LJF are warranted.

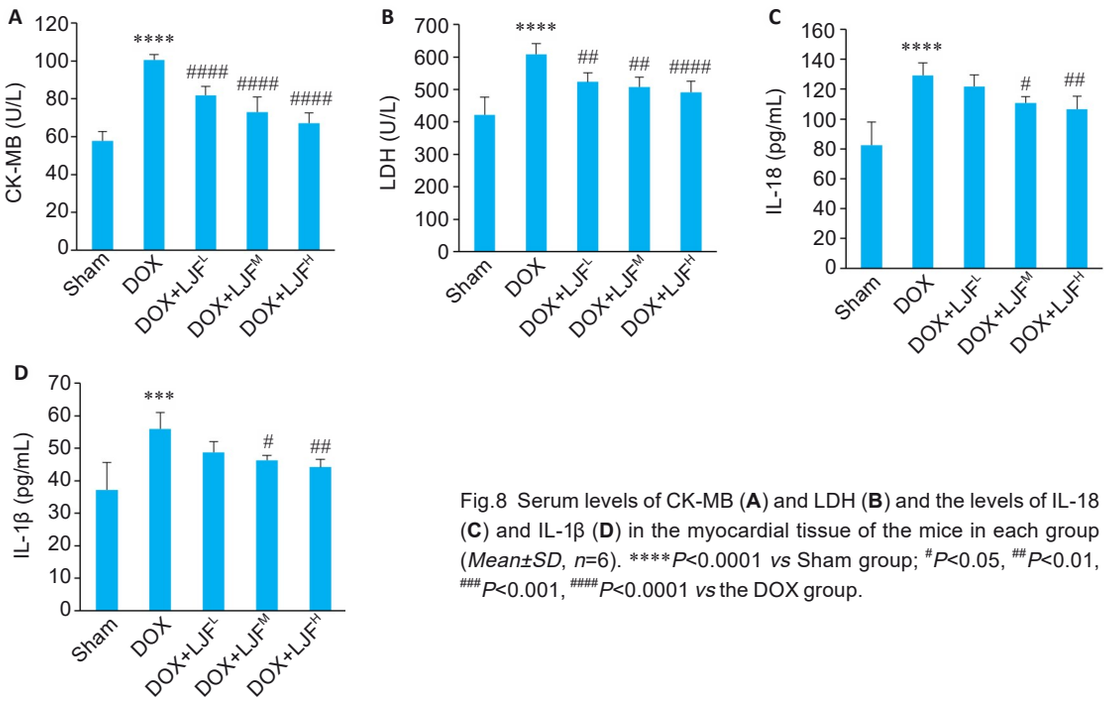

Fig.8 Serum levels of CK-MB (**A**) and LDH (**B**) and the levels of IL-18 (**C**) and IL-1β (**D**) in the myocardial tissue of the mice in each group (*Mean±SD*, *n*=6). ****P<0.0001 *vs* Sham group; $^{\#}P$<0.05, $^{\#\#}P$<0.01, $^{\#\#\#}P$<0.001, $^{\#\#\#\#}P$<0.0001 *vs* the DOX group.

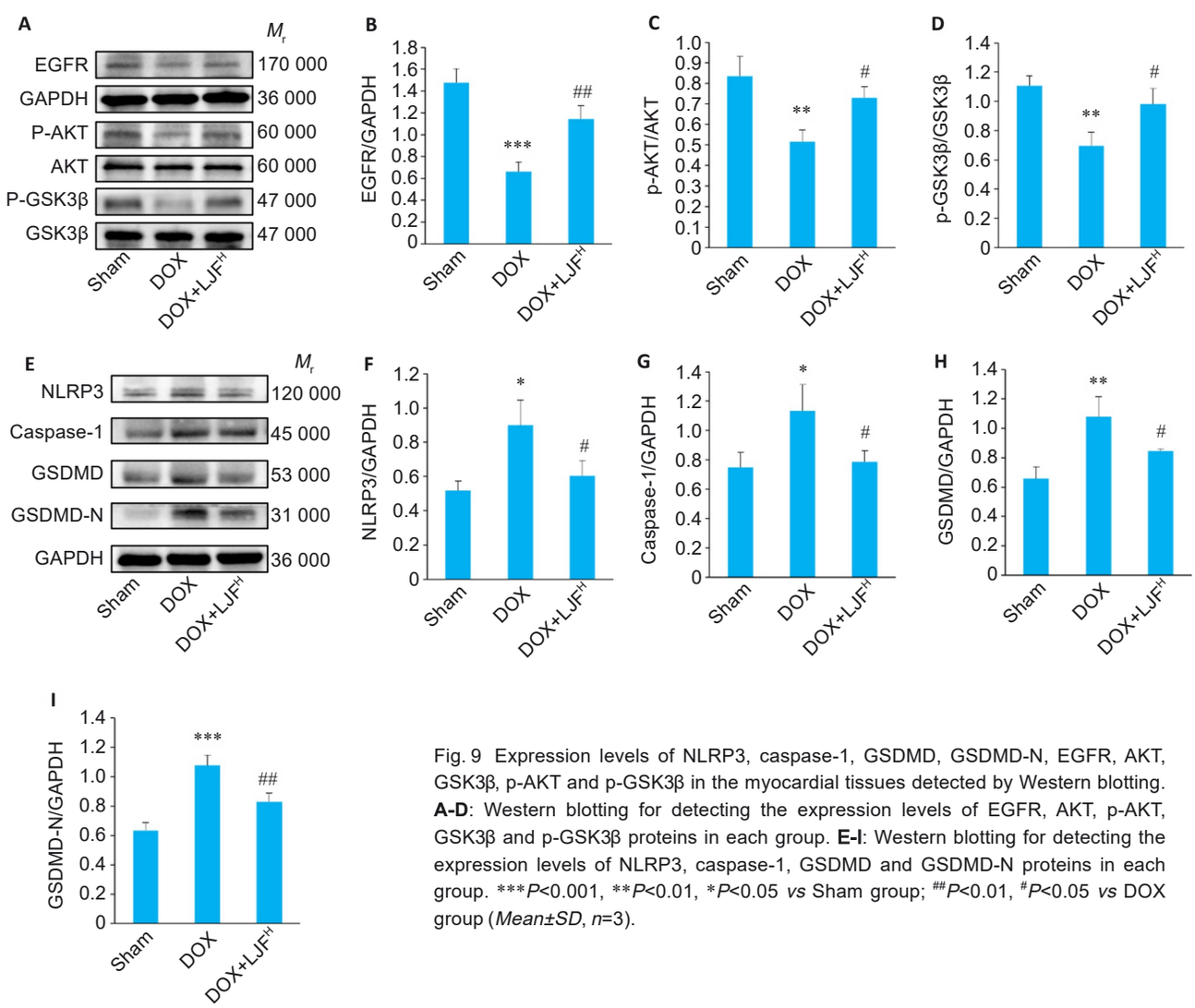

Fig. 9 Expression levels of NLRP3, caspase-1, GSDMD, GSDMD-N, EGFR, AKT, GSK3β, p-AKT and p-GSK3β in the myocardial tissues detected by Western blotting. **A-D**: Western blotting for detecting the expression levels of EGFR, AKT, p-AKT, GSK3β and p-GSK3β proteins in each group. **E-I**: Western blotting for detecting the expression levels of NLRP3, caspase-1, GSDMD and GSDMD-N proteins in each group. ***P<0.001, **P<0.01, *P<0.05 *vs* Sham group; $^{\#\#}P$<0.01, $^{\#}P$<0.05 *vs* DOX group (*Mean±SD*, *n*=3).

Declaration of interests: The authors declare no competing interests.

REFERENCES:

[1] Wang M, Xie D, Zhang M, et al. Multiple ingredients of a Chinese medicine formula Sheng-Mai-San coordinately attenuate doxorubicin-induced cardiotoxicity [J]. Pharmacol Res Mod Chin Med, 2023, 8: 100281.

[2] Powers SK, Duarte JA, Le Nguyen B, et al. Endurance exercise protects skeletal muscle against both doxorubicin-induced and inactivity-induced muscle wasting [J]. Pflugers Arch, 2019, 471(3): 441-53.

[3] Li D, Zhang W, Fu H, et al. DL-3-n-butylphthalide attenuates doxorubicin-induced acute cardiotoxicity via Nrf2/HO-1 signaling pathway [J]. Heliyon, 2024, 10(5): e27644.

[4] Chen M, Yi Y, Chen B, et al. Metformin inhibits OCTN1- and OCTN2-mediated hepatic accumulation of doxorubicin and alleviates its hepatotoxicity in mice [J]. Toxicology, 2024, 503: 153757.

[5] Badi RM, Khaleel EF, Satti HH, et al. Eriodictyol attenuates doxorubicin-induced nephropathy by activating the AMPK/Nrf2 signalling pathway [J]. J Tradit Complement Med, 2024, 14(2): 203-14.

[6] Qu Y. Gasdermin D mediates endoplasmic reticulum stress via FAM134B to regulate cardiomyocyte autophagy and apoptosis in doxorubicin-induced cardiotoxicity [J]. Cell Death Dis, 2022, 13(1): 1-12.

[7] Meng L, Lin H, Zhang J, et al. Doxorubicin induces cardiomyocyte pyroptosis via the TINCR-mediated posttranscriptional stabilization of NLR family pyrin domain containing 3 [J]. J Mol Cell Cardiol, 2019, 136: 15-26.

[8] Lai KH, Chen YL, Lin MF, et al. Lonicerae japonicae flos attenuates neutrophilic inflammation by inhibiting oxidative stress [J]. Antioxidants (Basel), 2022, 11(9): 1781.

[9] Zheng S, Liu S, Hou A, et al. Systematic review of Lonicerae Japonicae Flos: a significant food and traditional Chinese medicine [J]. Front Pharmacol, 2022, 13: 1013992.

[10] Wang L, Jiang Q, Hu J, et al. Research progress on chemical constituents of *Lonicerae japonicae flos* [J]. Biomed Res Int, 2016, 2016: 1-18.

[11] Han MH, Lee WS, Nagappan A, et al. Flavonoids isolated from flowers of *Lonicera japonica* Thunb. inhibit inflammatory responses in BV2 microglial cells by suppressing TNF-α and IL-β through PI3K/Akt/NF-κB signaling pathways [J]. Phytother Res, 2016, 30 (11): 1824-32.

[12] Bang BW, Park D, Kwon KS, et al. BST-104, a water extract of *Lonicera japonica*, has a gastroprotective effect via antioxidant and anti-inflammatory activities [J]. J Med Food, 2019, 22(2): 140-51.

[13] Wang T, Yang B, Guan Q, et al. Transcriptional regulation of *Lonicera japonica* Thunb. during flower development as revealed by comprehensive analysis of transcription factors [J]. BMC Plant Biol, 2019, 19(1): 198.

[14] Miao H, Zhang Y, Huang Z, et al. *Lonicera japonica* attenuates carbon tetrachloride-induced liver fibrosis in mice: molecular mechanisms of action [J]. Am J Chin Med, 2019, 47(2): 355-72.

[15] Li W, Zhang L, He P, et al. Traditional uses, botany, phytochemistry, and pharmacology of *Lonicerae japonicae* flos and *Lonicerae flos*: a systematic comparative review [J]. J Ethnopharmacol, 2024, 322: 117278.

[16] Yu P, Zhang X, Liu N, et al. Pyroptosis: mechanisms and diseases [J]. Signal Transduct Target Ther, 2021, 6(1): 128.

[17] Tao RH, Kobayashi M, Yang Y, et al. Exercise inhibits doxorubicin-induced damage to cardiac vessels and activation of hippo/YAP-mediated apoptosis [J]. Cancers, 2021, 13(11): 2740.

[18] Zhang G, Yang X, Su X, et al. Understanding the protective role of exosomes in doxorubicin-induced cardiotoxicity [J]. Oxid Med Cell Longev, 2022, 2022: 1-14.

[19] Ju YN, Zou ZW, Jia BW, et al. Ac2-26 activated the AKT1/GSK3β pathway to reduce cerebral neurons pyroptosis and improve cerebral function in rats after cardiopulmonary bypass [J]. BMC Cardiovasc Disord, 2024, 24: 266.

[20] Wei Y, Lan B, Zheng T, et al. GSDME-mediated pyroptosis promotes the progression and associated inflammation of atherosclerosis [J]. Nat Commun, 2023, 14: 929.

[21] Gong Y, Qiu J, Jiang T, et al. Maltol ameliorates intervertebral disc degeneration through inhibiting PI3K/AKT/NF-κB pathway and regulating NLRP3 inflammasome-mediated pyroptosis [J]. Inflammopharmacology, 2023, 31(1): 369-84.

[22] Zhou P, Song NC, Zheng ZK, et al. MMP2 and MMP9 contribute to lung ischemia-reperfusion injury via promoting pyroptosis in mice [J]. BMC Pulm Med, 2022, 22: 230.

[23] Yue L, Liu X, Wu C, et al. Toll-like receptor 4 promotes the inflammatory response in septic acute kidney injury by promoting p38 mitogen-activated protein kinase phosphorylation [J]. J Bioenerg Biomembr, 2023, 55(5): 353-63.

[24] Wang Y, Wei J, Zhang P, et al. Neuregulin-1, a potential therapeutic target for cardiac repair [J]. Front Pharmacol, 2022, 13: 945206.

[25] Wang X, Sun Q, Jiang Q, et al. Cryptotanshinone ameliorates doxorubicin-induced cardiotoxicity by targeting Akt-GSK-3β-mPTP pathway in vitro [J]. Molecules, 2021, 26(5): 1460.

[26] Yang K, Liu J, Zhang X, et al. H3 relaxin alleviates migration, apoptosis and pyroptosis through P2X7R-mediated nucleotide binding oligomerization domain-like receptor protein 3 inflammasome activation in retinopathy induced by hyperglycemia [J]. Front Pharmacol, 2020, 11: 603689.

[27] Huang L. The role of IL-17 family cytokines in cardiac fibrosis [J]. Front Cardiovasc Med, 2024, 11: 1470362.

[28] Liu W, Wang X, Wu W. Role and functional mechanisms of IL-17/IL-17R signaling in pancreatic cancer (Review) [J]. Oncol Rep, 2024, 52(5): 144.

[29] Hedhli N, Kalinowski A, Russell KS. Cardiovascular effects of neuregulin-1/ErbB signaling: role in vascular signaling and angiogenesis [J]. Curr Pharm Des, 2014, 20(30): 4899-905.

[30] Yenerall P, Das AK, Wang S, et al. RUVBL1/RUVBL2 ATPase activity drives PAQosome maturation, DNA replication and radioresistance in lung cancer [J]. Cell Chem Biol, 2020, 27(1): 105-21.e14.

[31] Andrei C, Zanfirescu A, Ni ulescu GM, et al. Natural active ingredients and TRPV1 modulation: focus on key chemical moieties involved in ligand-target interaction [J]. Plants, 2023, 12(2): 339.

[32] Zhang E, Yang Y, Chen S, et al. Bone marrow mesenchymal stromal cells attenuate silica-induced pulmonary fibrosis potentially by attenuating Wnt/β-catenin signaling in rats [J]. Stem Cell Res Ther, 2018, 9: 311.

[33] Xiao L, Qi L, Zhang G, et al. Polygonatum sibiricum polysaccharides attenuate lipopolysaccharide-induced septic liver injury by suppression of pyroptosis via NLRP3/GSDMD signals [J]. Molecules, 2022, 27(18): 5943.

[34] Rogers C, Fernandes-Alnemri T, Mayes L, et al. Cleavage of DFNA5 by caspase-3 during apoptosis mediates progression to secondary necrotic/pyroptotic cell death [J]. Nat Commun, 2017, 8: 14128.

[35] Chen X, Tian PC, Wang K, et al. Pyroptosis: role and mechanisms in cardiovascular disease [J]. Front Cardiovasc Med, 2022, 9: 897815.

[36] Ye B, Shi X, Xu J, et al. Gasdermin D mediates doxorubicin-induced cardiomyocyte pyroptosis and cardiotoxicity via directly binding to doxorubicin and changes in mitochondrial damage [J]. Transl Res, 2022, 248: 36-50.

[37] Chai R, Li Y, Shui L, et al. The role of pyroptosis in inflammatory diseases [J]. Front Cell Dev Biol, 2023, 11: 1123456.

（编辑：宋建武）

金银花提取物对阿霉素诱导的小鼠心肌损伤的保护作用及其机制

夏士程[1,3],韦慧芳[1,3],洪维灿[1,3],张钰明[2,3],尹菲玥[1,3],张贻欣[1,3],张淋淋[2,3],高 琴[2,3],叶红伟[2,3]
蚌埠医科大学[1]临床医学院,[2]生理学教研室,[3]心脑血管疾病基础与临床重点实验室,安徽 蚌埠 233030

摘要:目的 探讨金银花(LJF)对阿霉素(DOX)诱导的心肌损伤的保护作用及其机制。**方法** 通过网络药理学、生物信息学分析与分子对接技术预测核心靶点,并通过动物实验加以验证。动物实验中,检测DOX诱导的心肌损伤及不同剂量LJF提取物治疗后小鼠心功能、心肌酶学、心肌组织形态、炎症因子及相关蛋白表达的变化。**结果** 网络药理学筛选出LJF的10个核心活性成分可与AKT、EGFR、GSK3β良好结合。动物实验结果显示,与假手术组相比,DOX组小鼠心输出量、每搏输出量、左室射血分数及左室短轴缩短率显著降低,血清CK-MB、LDH水平升高,心肌IL-18、IL-1β含量增加;HE染色示心肌结构损伤;心肌组织NLRP3、caspase-1、GSDMD及GSDMD-N蛋白表达上调,EGFR蛋白表达下调,p-AKT、p-GSK3β蛋白水平降低。与DOX组相比,LJF治疗后小鼠心功能明显改善,心肌组织中IL-18、IL-1β水平降低,NLRP3、caspase-1、GSDMD及GSDMD-N蛋白表达下调,EGFR蛋白水平上调,p-AKT、p-GSK3β蛋白磷酸化水平提高。**结论** 金银花可能通过靶向作用于EGFR、AKT、GSK3β调控ErbB信号通路,抑制心肌组织炎症反应与细胞焦亡,从而减轻阿霉素诱导的心肌损伤。

关键词:网络药理学;金银花提取物;阿霉素;分子对接;细胞焦亡;ErbB信号转导通路

收稿日期:2025-03-04

基金项目:安徽省高校优秀科研创新团队项目(2022AH010083);蚌埠医科大学"512人才计划"(by51201102);大学生创新创业训练计划项目(S202410367081,S202410367011,202410367058,S202410367057)

作者简介:夏士程,本科,E-mail:12210110342@stu.bbmc.edu.cn

通信作者:叶红伟,硕士,副教授,E-mail:yehongwei223@163.com;高 琴,博士,教授,E-mail:bbmcgq@126.com